Acta Oceanol. Sin., 2017, Vol. 36, No. 9, P. 65–78
DOI: 10.1007/s13131-017-1112-1
http://www.hyxb.org.cn
E-mail: hyxbe@263.net

Basin modeling in the initial stage of exploration: a case study from the North Subbasin of the South Yellow Sea Basin

PANG Yumao[1, 2, 3, 4], ZHANG Xunhua[2, 4, 5*], GUO Xingwei[2, 4], XIAO Guolin[2, 4], HAN Zuozhen[1]

[1] College of Earth Science and Engineering, Shandong University of Science and Technology, Qingdao 266590, China

[2] Laboratory for Marine Mineral Resources, Qingdao National Laboratory for Marine Science and Technology, Qingdao 266071, China

[3] Institute of Oceanology, Chinese Academy Science, Qingdao 266071, China

[4] Qingdao Institute of Marine Geology, Qingdao 266071, China

[5] Nanjing Center, China Geological Survey, Nanjing 210016, China

Received 5 February 2017; accepted 21 March 2017

Abstract

Basin modeling has become an important tool for analyzing sedimentary basins. The North Subbasin of the South Yellow Sea Basin is filled with thick Meso-Cenozoic terrigenous deposits during the rift evolution stage. The accumulation of data and achievements of geological investigations in recent years have provided the preconditions for basin modeling. The necessary parameters and geological elements for simulations are collated and summarized. Modeling of tectono-thermal evolution is performed and the related trend in heat flow is reconstructed and calibrated. The heat flow value commences from an average level of 61 mW/m^2 during Middle-Late Jurassic, rises to about 80 mW/m^2 from circa 145 Ma to circa 74 Ma, and then undergoes a gradual decline to 65 mW/m^2 until the end of Oligocene.Three evolutionary phases, namely, the initial rifting phase, syn-rifting phase, and post-rifting phase, have been identified. The modeling results show that the North Subbasin generally enters into a stage of strong rifting during Cretaceous and undergoes rapid subsidence until the Late Cretaceous, then follows by a stage of moderate rifting during the Paleogene. The input and general workflow involved in 3-D modeling are introduced. Reconstruction of the petroleum system in the North Subbasin reveals that the threshold depth of hydrocarbon generation is located near the top of the Paleogene Funing formation, and the underlying Jurassic and Cretaceous source rocks have reached or exceeded peak oil generation and have almost completed the generation and expulsion of hydrocarbons. The main generation and expulsion in the Jurassic source rocks take place during the syn-rifting and post-rifting phases, whereas the peak generation and expulsion in the Cretaceous and Paleogene source rocks take place during the post-rifting phase. Although the study area is still a relatively less explored sedimentary basin, the results of modeling can provide valuable information for exploration. A preliminary discussion of the main uncertainty factors is also presented.

Key words: basin modeling, tectono-thermal evolution history, petroleum system, South Yellow Sea Basin

Citation: Pang Yumao, Zhang Xunhua, Guo Xingwei, Xiao Guolin, Han Zuozhen. 2017. Basin modeling in the initial stage of exploration: a case study from the North Subbasin of the South Yellow Sea Basin. Acta Oceanologica Sinica, 36(9): 65–78, doi: 10.1007/s13131-017-1112-1

1 Introduction

Basin modeling is an effective way to investigate the petroleum system in sedimentary basins (Poelchau et al., 1997; Schneider et al., 2000; Rodriguez and Littke, 2001; Pitman et al., 2004; Baur et al., 2010; Welte and Yalçin, 1988). As a finite-element-based forward modeling technology, it can be performed using some standard, commercially available software tools. The overall goal of basin modeling is to simulate and reconstruct the burial and thermal evolution history of sedimentary basins, as well as the geodynamic processes in petroleum systems such as the maturation of organic matter and the generation, expulsion, migration, accumulation, and preservation of hydrocarbons (Wygrala, 1988; Yalçin, 1991; Magoon and Dow, 1994; Waples, 2001; Poelchau et al., 1997; Gonçalves et al., 2002; Baur et al., 2010). In the initial stage of hydrocarbon exploration, basin modeling is an effective method of assessing the exploration risks. It can simulate geodynamic processes in petroleum systems, which are linked to the complex evolution of basins with changeable geological settings during their long geological history (Poelchau et al., 1997).

The South Yellow Sea Basin is a large-scale superimposed sedimentary basin comprising pre-Indosinian marine craton deposits and Meso-Cenozoic terrigenous deposits (Zhang et al., 2014a; Pang et al., 2016a). It underwent strong rift-dominated sedimentation during the Meso-Cenozoic and was filled with thick terrigenous deposits (Yi et al., 2003; Wu et al., 2008; Pang et al., 2016b). Previous regional geological investigations and explorations have so far revealed some fundamental characteristics of the petroleum system such as the geochemical features of the source rocks, stratigraphic framework, and potential reser-

Foundation item: The National Special Project for Marine Geology of China under contract No. DD20160147; the National Basic Research Program (973 Program) of China under contract No. 2013CB429701; the National Natural Science Foundation of China under contract No. 41210005.

*Corresponding author, E-mail: xunhuazh611102@sina.com

voirs and shown great resource potential in the South Yellow Sea Basin (Xiao, 2002; Wu et al., 2008; Yao et al., 2008; Pang et al., 2016a). Nearly half of the South Yellow Sea Basin is surrounded by the eastern China petroliferous basins, including the Songliao, Bohai Gulf, Subei, and East China Sea basins, most of which have already shown great hydrocarbon resource potential (Li et al., 2003, 2009; Zhang et al., 2006). However, as a relatively less explored petroleum-bearing basin, the integrated investigation of the petroleum system in this basin has lacked study until now, which has restricted the progress of the petroleum exploration. In this study, we concentrate on the North Subbasin of the South Yellow Sea Basin and focus on the investigation of the geological elements associated with the petroleum system. For this purpose, tectono-thermal evolution modeling and preliminary 3-D numerical simulations have been performed. The methodology of basin modeling is also an important part of this study, and the related preparation of data and simulation workflow, as well as key approaches to the control of parameters, are introduced.

2 Geological setting

The South Yellow Sea Basin, which is located on the continental shelf offshore from the Lower Yangtze Block of eastern China, is a continental margin basin (Pang et al., 2017). On the basis of the Meso-Cenozoic fault-bounded sedimentary area of the basin and the gravity anomaly characteristics, it can be roughly subdivided into five secondary units from north to south (Zhang et al., 2007, 2014a; Yao et al., 2008): the Qianliyan uplifted zone; northern South Yellow Sea depression, also called the North Subbasin; central uplifted zone; South Subbasin; and Wunansha uplifted zone. Controlled by faults trending NE-SW or E-W, the substructural units generally have strikes trending NE-SW and E-W. The uplifted zones and depressions have similar marine sedimentary basements, whereas Meso-Cenozoic terrigenous sediments mainly occur in subbasins and/or depressions, e.g., the North Subbasin. There is a remarkable absence of Meso-Cenozoic deposits in the central uplifted zone, as proved by drilling wells and seismic data, which shows that the Neocene deposits directly overlie Triassic or Paleozoic strata.

The North Subbasin is a typical Meso-Cenozoic rifted subbasin with several depressions, and the depth of the depocenter can reach 9 000 m (Fig. 1). It is bounded by deep faults trending N-E and NE-E to the north and the south, is surrounded by the Paleozoic basement in the east and the west, and covers an area of approximately 50 000 km^2 (Xiao, 2002; Gao et al., 2015). In a NE-SW direction, the North Subbasin can be subdivided into four segments (marked as A, B, C, and D in Fig. 1), which are bounded by faults trending NE-SW and E-W (Fig. 1).

In the North Subbasin, Meso-Cenozoic sediments rest upon the underlying marine cratonic sedimentary rocks (Fig. 2). Several hiatuses and unconformities, which resulted from regional tectonic events, have been recognized and confirmed according to the results of drilling wells and related seismic tracking. In comparison with the relatively continuous stratigraphic sequences in depression areas, hiatuses mainly developed in the uplifted zones. Thick continental clastic sediments were formed during the Meso-Cenozoic, providing the substantial fundamental elements of the petroleum system. There are several sets of potential source-reservoir-cap rock assemblages in the Meso-Cenozoic sedimentary intervals (Fig. 2) (Xiao, 2002; Yi et al., 2003; Yao et al., 2008, 2010; Qi et al., 2013; Pang et al., 2016a). The results of drilling have revealed that the dark mudstones of the upper Cretaceous Taizhou formation (K_T) and the Paleogene Funing formation (E_F) are two sets of important potential source rocks (Zhu, 2007). In comparison with the limited distribution of Jurassic strata, Cretaceous strata are widespread, and the depocenter can reach a depth of 2 000 m (Figs 1 and 2). The dark mudstone of the upper K_T (in the Segments B, C, and D in Fig. 1), which was formed in a lacustrine environment, is mainly a type II kerogen with a total organic carbon (TOC) content ranging from 0.59% to 0.92%, and its total hydrocarbon content can range from 237 to 837 mg/kg. This set of dark mudstones can serve as good source rocks. The Cretaceous strata in the northeastern segment (Segment A), by contrast, are characterized by red clastic strata, which were encountered by the Haema-1 well (Xiao, 2002; Yi et al., 2003); hence, it cannot serve as a source rock. The E_F mainly comprises fluvial-lacustrine sand/shale interbeds. The lacus-

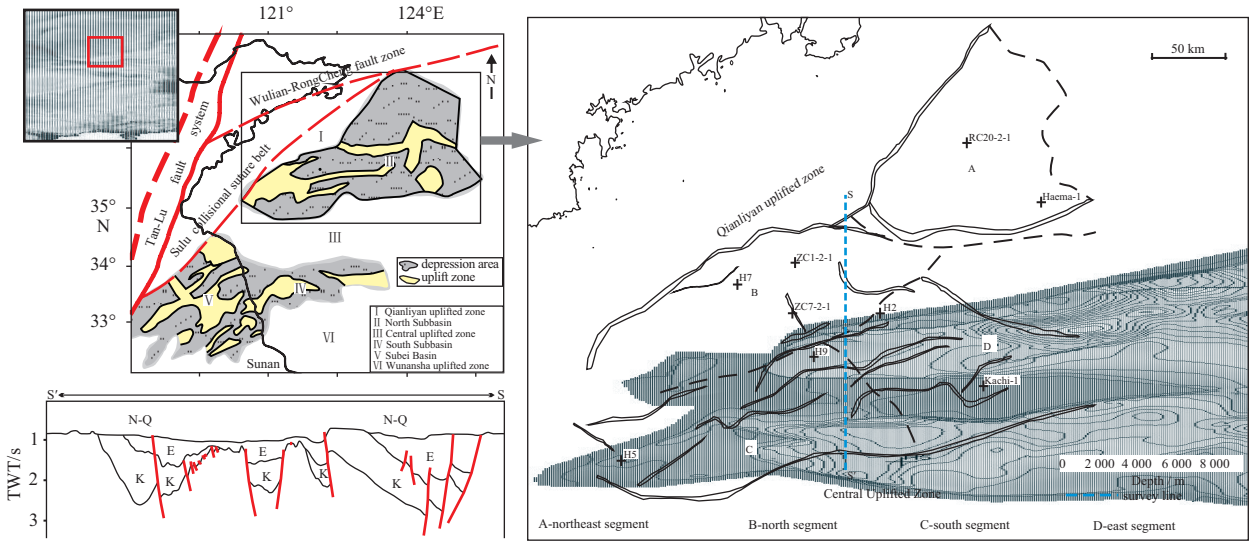

Fig. 1. Maps of the location and structural outline of the North Subbasin. The profile in the N-S direction is derived from the interpretation of the results of multichannel seismic data. The main faults are drawn according to the interpretation of the results of 2-D seismic data by the Qingdao Institute of Marine Geology (QIMG). The black plus signs show the positions of key wells (modified after Zhang et al., 2014b), which were used as important calibration data for the numerical stratigraphic framework.

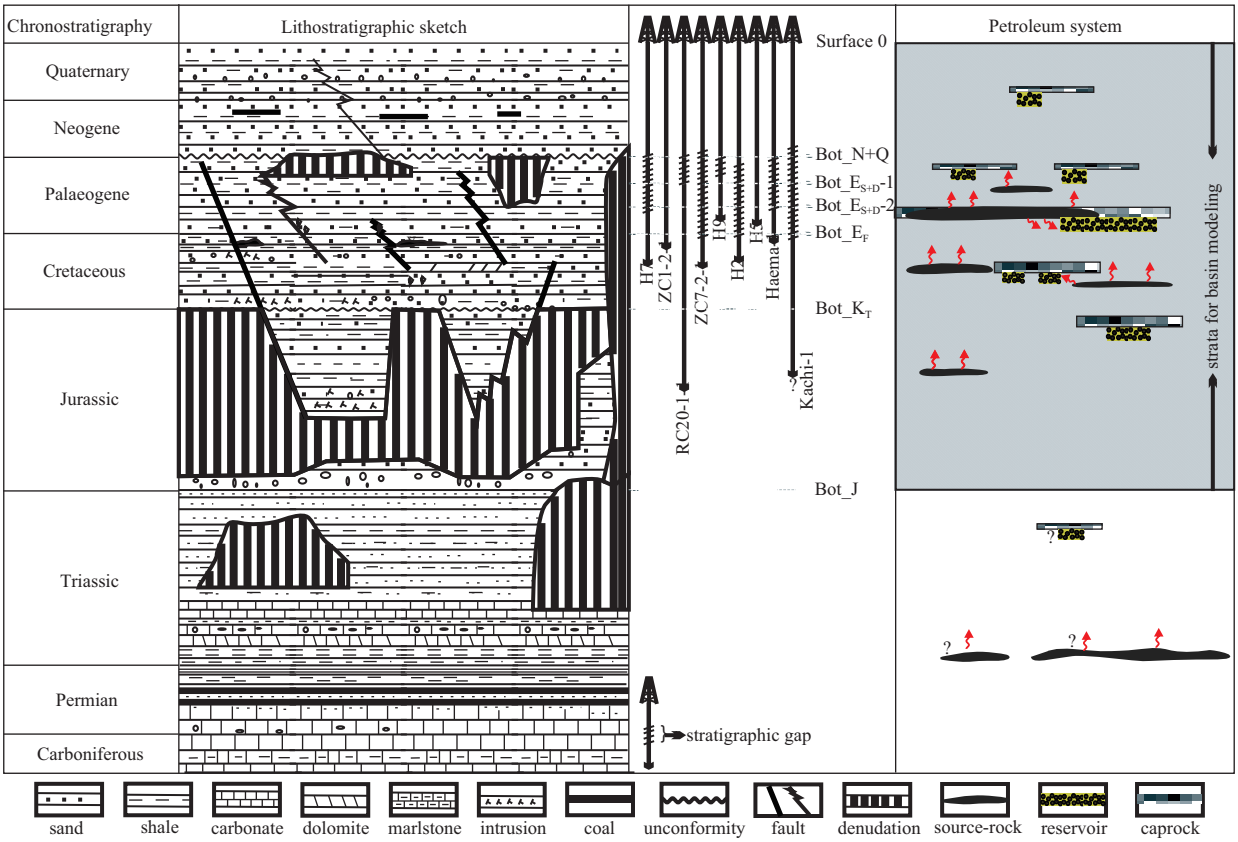

Fig. 2. Chronostratigraphic chart and elements of the petroleum system of the North Subbasin based on a database of the South Yellow Sea Basin and the results of previous research (Yao et al., 2010; Pang et al., 2016a). The six structural depth maps (Bot_N+Q; Bot_E$_{S+D}$-1; Bot_E$_{S+D}$-2; Bot_E$_F$; Bot_K$_T$; and Bot_J) were derived from wells and seismic surveys (2-D seismic only), which were integrated by QIMG.

trine dark mudstone is a type II/III kerogen; its TOC content ranges from 0.57% to 1.91%, and its total hydrocarbon content can reach 1 038 mg/kg. In addition, the RC20-2-1 well encountered Jurassic strata at a depth of more than 2 000 m in the northeastern segment. The upper part of the Jurassic strata is mainly a fluvial sedimentary formation, whereas the lower part is characterized by thick lacustrine dark mudstones, which have good hydrocarbon generation potential and can also be well correlated with the Jurassic source rocks in the North Yellow Sea Basin (Gao and Zhou, 2014). The dark mudstone intervals in the Paleogene Dainan formation are generally immature. According to the regional geological correlation and results of current drilling, beneficial reservoir-seal associations have mainly developed in the intervals of Cretaceous and Paleogene strata (Xiao, 2002; Pang et al., 2016a). The pattern of the petroleum system in the intervals of the Meso-Cenozoic strata in the North Subbasin is illustrated in Fig. 2.

The faults that developed under the extensional background are significant pathways for the vertical migration of petroleum. In the North Subbasin, many Meso-Cenozoic faults have been identified on the basis of 2-D seismic data (Gao et al., 2015). Some basin-controlling faults are shown in Fig. 1 and their spatial distribution patterns are sketched in Fig. 2. The Middle-Late Jurassic period is the key stage when the South Yellow Sea Basin gradually entered into the initial stage of the evolution of an extensional basin. Some syn-rifting normal faults began to develop, accompanied by the structural reversion of some previous compressive faults (Hou et al., 2008; Pang et al., 2016b). In general, this extensional fault system developed continuously from the Early Cretaceous to the Late Oligocene. Since the Early Miocene, the basin has experienced regional subsidence, thus entering into the stage of evolution to form a depression (Yao et al., 2005; Hou et al., 2008; Qi et al., 2013; Pang et al., 2016b). Except for a few inherited boundary faults, most faults mainly develop below the Miocene surface, which is a regional unconformity surface.

3 Methods and data

The modeling processes were performed with IES PetroMod software (2012), which can provide a standardized user interface across the entire 1-D, 2-D, and 3-D software suite. Related gridding of surfaces was performed with Petrel software (2009) from Schlumberger. As a finite-element-based forward modeling technolog, the main workflow of basin modeling includes the following procedures (Novelli et al., 1988; Poelchau et al., 1997; Schneider et al., 2000; Baur et al., 2010): (1) determination of the geological framework of the basin, such as its fault system, lithostratigraphic framework, sedimentary facies, and structural characteristics; (2) collation of the results of research into the petroleum system, i.e., the source rocks, reservoir intervals, and potential cap rocks, and the evaluation of these results based on the measured data; (3) design and construction of a conceptual model for dividing the evolutionary history of the basin into a series of events for marking the present layers; (4) preparation of input and calibration data, i.e., well data, facies data, surfaces from seismic data, erosion maps, fault data, geochemical parameters, and geothermal and hydrodynamic data, boundary con-

ditions such as the paleo-water depth (PWD), sediment-water interface temperature (SWIT), and heat flow (HF) should be determined on the basis of the available geological data before modeling; (5) 1-D modeling of the representative wells to confirm the validity of the conceptual model of the basin and iterative calibration to optimize the input data, particularly the boundary conditions for complex 3-D modeling; (6) integrated 3-D numerical modeling, including the construction of a geological model, setting of parameters, and simulation; (7) testing and comparison of the output with the measured data from samples; and (8) discussion of the results and analysis of uncertainty.

To meet the data requirements of basin modeling, the latest results of seismic interpretation such as basin boundary lines, surfaces, erosion data, and fault lines were collected from the Basin Database (BHH) of the Qingdao Institute of Marine Geology (QIMG). Information on the progress of some regional geological research and related data are available from the published literature, which has been indicated in the corresponding locations. Several representative seismic sections such as the S-S' section shown in Fig. 1 were obtained and reinterpreted to constrain the stratigraphic model. Calibration of horizons and stratigraphic correlation were performed on the basis of several wells with good well ties such as H2, H7, and Kachi-1. Geophysical and geochemical parameters of different lithologies for assigning the gridding cells were derived from various sources, including the measured data from drilling samples, published data, and comparative data for the corresponding strata in an adjacent area.

4 Modeling of tectono-thermal evolution

4.1 *Principles and general workflow*

Basins are generally classified according to their plate tectonic position (Helwig, 1985; Allen and Allen, 1990; Poelchau et al., 1997). The South Yellow Sea Basin is a back-arc extensional sedimentary basin formed during the Meso-Cenozoic (Yi et al., 2003; Lee et al., 2006; Pang et al., 2016b). The tectono-thermal evolution modeling is one of the foundations of the modeling of extensional basins. This study used the forward modeling method and employed PetroMod basin-modeling software to combine the analysis of the basin dynamics with the modeling of the petroleum system (Baur et al., 2010). With the current geothermal data as constraining conditions, the tectono-thermal evolution history of the study area was recovered both on the lithosphere and basin scale. This method was developed from the limited extension rate model (Jarvis and McKenzie, 1980), which is based on the model of instantaneous uniform pure-shear tension proposed by McKenzie (1978). At the extension stage, not only tectonic subsidence caused by thinning of the lithosphere but also subsidence caused by a thermal relaxation effect in the lithosphere were taken into consideration; hence, the method can be well matched with the 1-D back-stripping technology. Moreover, heat loss and thermal subsidence in the post-rifting period were considered during the modeling process. The contribution of the radioactive generation of heat in the crust was also superimposed.

The process is summarized as follows:

Step 1. Based on the present-day geometry, the age assignment and defined erosions by stepwise decompaction of the sediments, the Airy theory of isostatic compensation, and the back-stripping method proposed by Steckler and Watts (1978) were employed for the back-stripping equation to calculate the burial history and theoretical trend in tectonic subsidence.

Step 2. The stretching factors are determined by applying a stretching model. The corresponding geophysical parameters were set and the stretch factors were constantly adjusted to calculate the best-fit between the theoretical and calculated tectonic subsidence curves. Accordingly, the stretch factors are used to develop the heat flow history by applying the stretching model again. Then the calibration of the stretch factors should be performed. First, on the basis of the definition of stretch factor, the initial thickness of the crust and the stretch factor were used to determine the current calculated thickness of the crust, which was confirmed by comparison with the actual thickness of the crust. Next, the measured thermometric data were used to calibrate the thermal history trend.

Step 3. The thermal history obtained by the 1-D modeling and the related parameters were used as 3-D input to simulate the paleo-geothermal field and the petroleum system.

4.2 *Data input*

Modeling of the tectono-thermal evolution was performed for several representative well locations to reconstruct the history of their tectono-thermal evolution. On the basis of the BHH and published data (Yi et al., 2003; Gao and Zhou, 2014; Zhang et al., 2014b), the stratigraphy, lithostratigraphy, and calibration data were input into the 1-D module. The fine strata were depicted according to the generalized geogram of a single well, in which the thickness from the well bottom to the bottom boundary of the downfaulted sedimentary basin was calculated by the interpretation of the multichannel seismic data. Lithological, geophysical, and geochemical parameters were set by the combination of data from the PetroMod standard-based rock sample library (Table 1), where the values of average thermal conductivity refer to the measured samples from the South Yellow Sea Basin and the data from adjacent regions (Wang et al., 1995; Yang et al., 2003a, b). The settings for other related constraining conditions and parameters such as the crustal thickness, mantle thickness, and corresponding density and temperature on the bottom of the lithosphere are listed in Table 2. Some data refer to the research results of the Subei Basin on land (Bao et al., 2013a, b).

The PWD was mainly deduced by the analysis of sedimentary facies and biostratigraphy (Yi et al., 2003; Cao and Ye, 2008; Cai et al., 2014; Zhang et al., 2014b). The values for the lacustrine dark mudstone group, light gray mudstone group, and sandstone group were set at 20, 10, and 3 m, respectively. The SWIT was calculated from the global mean surface temperature (Wygrala, 1989), and the paleo-latitude was set at 35°N.

4.3 *Parameter calibration*

In the modeling process, the trend in subsidence and the theoretical trend in tectonic subsidence were first calculated by fitting to each other to obtain the corresponding stretch factor. Taking the ZC1-2-1 well as an example, the stretch factor was determined via fitting calculations of the trend in subsidence and the theoretical trend in tectonic subsidence [β(crust)=1.21, γ(mantle)=1.49] (Fig. 3). The initial crust-mantle thickness has a significant impact on the calculation of the tectonic subsidence curve (Liu and He, 2015). After the crust-mantle stretch factor was obtained, the current calculation-based crust-mantle thickness was compared with the measured value to test the validity of the initial crust-mantle thickness and the corresponding stretch factor. The reference values of the measured crust thickness were 28.5–30.0 km in the western part of the Yellow Sea and around 29 km in the eastern part of the Yellow Sea (Xu et al., 2009). On the basis of the balanced section method, previous studies have conducted similar research on the Subei Basin in the lower Yangtze

Table 1. List of basic parameters of different rock types for modeling of tectono-thermal evolution

Lithology	Mechanical compaction (Athy's law)			Thermal conductivity (Sekiguchi model)		Radiogenic heat			
	Grain density/ $kg\cdot m^{-3}$	Initial porosity (Φ)/ %	Athy's factor/ km^{-1}	Thermal conductivity/ $W\cdot m^{-1}\cdot K^{-1}$ T=20/100/200°C	Anisotropy factor	Uranium/ 10^{-6}	Thorium/ 10^{-6}	Potassium/ 10^{-6}	Heat flow production/ $\mu W\cdot m^{-3}$ Φ=20%/40%
Shale (black)	2 500	70	0.83	0.90/1.15/1.35	3.27	19.0	11.00	2.50	4.35/3.27
Shale (organic rich)	2 600	70	0.83	1.25/1.41/1.53	2.19	5.00	12.00	2.80	1.83/1.37
Shale (organic lean)	2 700	70	0.83	1.70/1.74/1.77	1.55	3.70	12.00	2.70	1.63/1.22
Sandstone (typical)	2 720	41	0.31	3.95/3.38/2.95	1.15	1.30	3.50	1.30	0.56/0.42
Sandstone (clay rich)	2 760	40	0.32	3.35/2.95/2.63	1.20	1.50	5.10	3.60	0.88/0.66
Sandstone (clay poor)	2 700	42	0.30	5.95/4.85/4.00	1.05	0.70	2.30	0.60	0.32/0.24
Siltstone (organic lean)	2 720	55	0.51	2.05/1.99/1.95	1.5	2.00	5.00	1.00	0.77/0.58
Siltstone (organic rich)	2 710	55	0.51	2.01/1.96/1.93	1.71	2.00	5.00	1.00	0.77/0.57
Limestone	2 740	51	0.52	3.00/2.69/2.45	1.19	1.00	1.00	0.20	0.28/0.21
Dolomite	2 790	35	0.39	4.20/3.57/3.08	1.06	0.80	0.60	0.40	0.24/0.18
Sh50Ss50①	2 710	55	0.57	2.55/2.36/2.21	1.36	2.50	7.75	2.00	1.10/0.82
Sh80Ss20①	2 704	64	0.73	1.96/1.93/1.90	1.50	3.22	10.30	2.42	1.42/1.06
Sh60Ss20Sis20①	2 708	61	0.66	2.09/2.02/1.97	1.45	2.88	8.90	2.08	1.24/0.93
Sh5Ss95①	2 719	42	0.34	3.78/3.26/2.86	1.17	1.42	3.92	1.37	0.62/0.46
Sh90Sis5Ss5①	2 702	67	0.79	1.73/1.76/1.78	1.57	3.50	11.23	2.54	1.53/1.15
Sh30Sis70①	2 714	59	0.61	1.92/1.90/1.88	1.53	2.51	7.10	1.51	1.03/0.77
Sh10Ss20Ds70①	2 767	40	0.42	3.78/3.26/2.86	1.12	1.19	2.32	0.81	0.44/0.33
Sh5Ls10Ds85①	2 780	38	0.43	3.87/3.33/2.91	1.09	0.97	1.21	0.50	0.31/0.23
Sh20Ss80①	2 716	47	0.41	3.31/2.92/2.61	1.23	1.78	5.20	1.58	0.78/0.58
Sh80Ss15Ls5①	2 705	65	0.74	1.93/1.91/1.89	1.50	3.21	10.18	2.36	1.40/1.05
Sh85Sis15①	2 703	68	0.78	1.70/1.74/1.77	1.58	3.44	10.95	2.44	1.50/1.12
Ls70Ds30①	2 755	46	0.48	3.32/2.92/2.62	1.15	0.94	0.88	0.26	0.27/0.20
Rhyolite	–	–	–	2.60/2.40/2.24	1.20	5.80	13.00	3.70	2.03/1.52
Tuff	–	–	–	2.55/2.36/2.21	1.00	0.00	12.00	2.50	0.88/0.66

Note: The lithology is based on Yi et al.(2003), and ① values for these lithologies are taken from Hantschel and Kauerauf (2009), other values are determined by linear interpolations for the mixing to creat user-defined lithologies in PetroMod 2012. Different rock types have been simplified by Sh_Shale/Ss_Sandstone/Sis_Siltstone/Ls_Limestone/Ds_Dolomite.

Table 2. Geophysical properties of the crust and mantle

Geophysical parameters	Values
Initial crustal thickness/km	28.5–32.0
Lithosphere thickness/km	≈125
Lithospheric mantle thickness/km	92–95
Asthenosphere temperature/°C	1 333
Thermal conductivity@20/100°C/$W\cdot m^{-1}\cdot K^{-1}$	2.60/2.40-crust
	4.00/3.42-mantle
Crustal density/$kg\cdot m^{-3}$	2 870
Lithospheric mantle density/$kg\cdot m^{-3}$	3 200
Sedimentary water density/$kg\cdot m^{-3}$	1 040

Note: Data of lithospheric structure are based on Xu et al. (2008), Xu et al. (2009), Hao (2010) and research report of the serial maps of geology and geophysics in China's seas and their adjacent area. The thermophysical parameters are based on Baur et al. (2010), He (2002) and Liao et al. (2011).

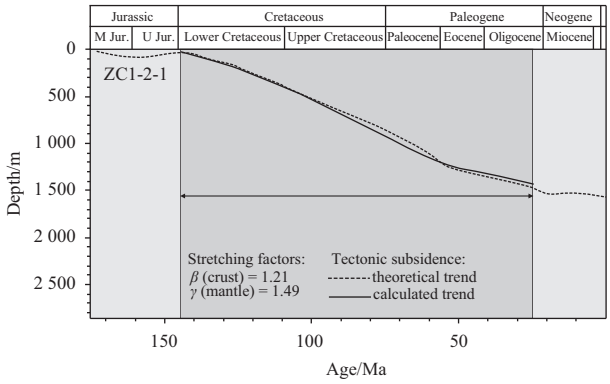

Fig. 3. Fitting results for tectonic subsidence derived from the ZC1-2-1 well and related stretching factors.

region (Bao et al., 2013a) and concluded that the stretch factor for the Subei Basin since the Cretaceous period was around 1.1–1.4, whereas the numerical modeling-based stretch factor for the North Subbasin of the South Yellow Sea was 1.15–1.5. Both factors were roughly the same, which confirmed that this method could be applied for the study of the tectono-thermal evolution of such basins.

The measured geothermal data were used for the calibration of the results of modeling on a basin scale. Considering the ZC1-2-1 and H9 wells, which provided relatively complete data, in the study area as examples, the trend in HF calculated by numerical modeling served as the initial value. The initial trend in HF that was assigned in the model was constrained by the results of the study by Qiu (2004), which were calibrated by comparing measured and calculated temperature-sensitive parameters, e.g., vitrinite reflectance. According to research into the geological conditions and HF in the lower Yangtze region and adjacent regions (Wang et al., 1995; Yang et al., 2003a, b ; Qiu, 2004), the current value of HF is about 65 mW/m^2, which is slightly higher than the average value of 61 mW/m^2 for the global land area. Therefore, the fluctuation interval of the current value of HF was set at 62–66

mW/m^2. The EASY*Ro*(%) model was used for modeling calculations to obtain the corresponding *Ro* depth curve (Sweeney and Burnham, 1990), and then the measured *Ro* data were used for the calibration of the trend in HF to obtain the calibrated ideal trend line for HF (Fig. 4). The measured *Ro* data from the ZC1-2-1 and H9 wells were mainly derived from the lower and central parts of the Funing formation and the Sanduo and Dainan formations. The combined constraints can be used for the effective calibration of the geothermal history on a basin scale since the post-rifting period in the Eocene (Fig. 4).

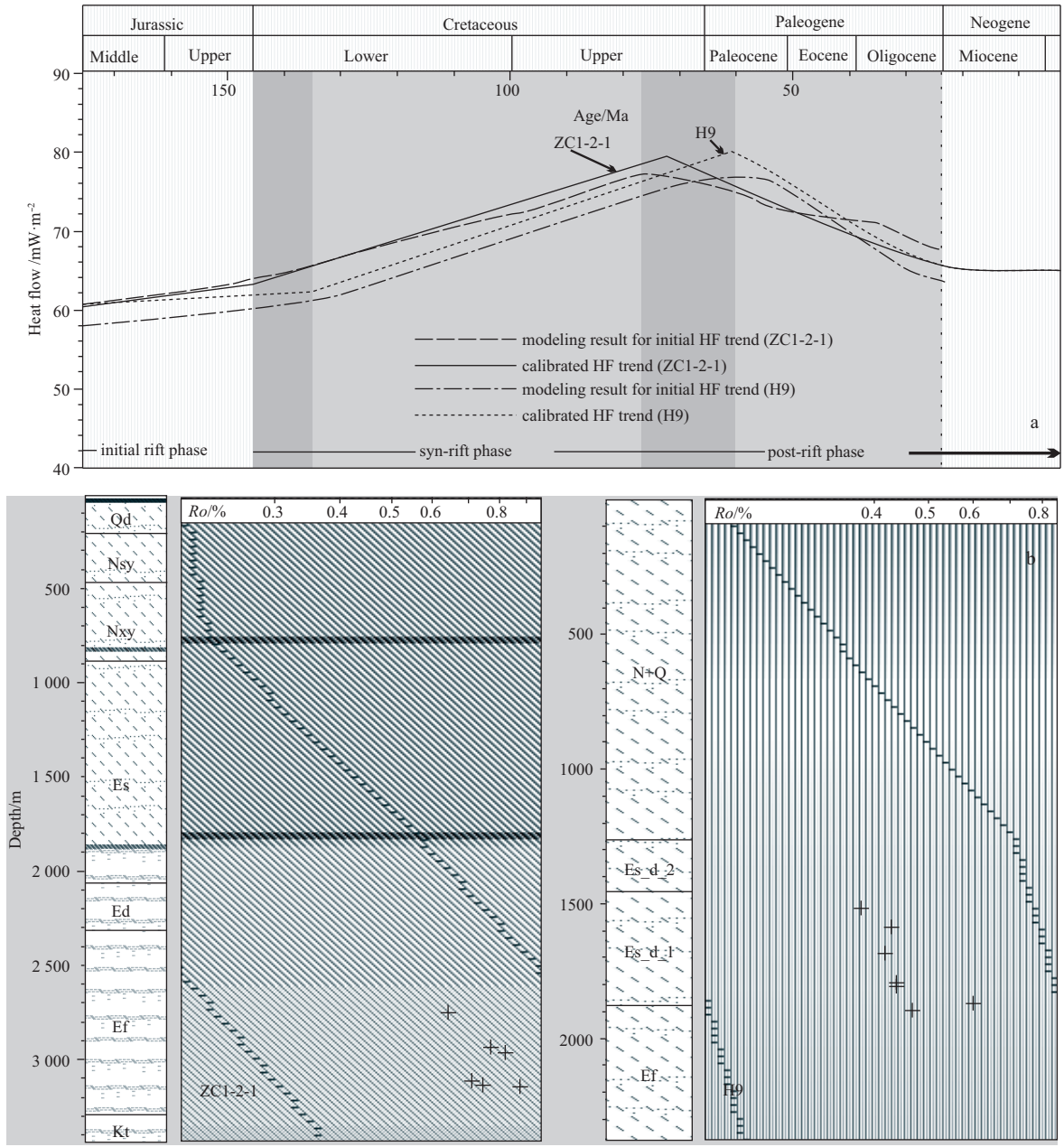

Fig. 4. Trends in heat flow (HF) for two single boreholes are calibrated by the measured data. The ZC1-2-1 well is located near the depocenter of the northern segment, and the H9 well is located in the transitional uplifted area; their locations are marked in Fig. 1. The initial trend in HF is derived from the modeling results (Fig. 4a). The final calibrated HF trends can provide more reasonable Ro evolutionary curves, which match the measured data *Ro*(%) well (Fig. 4b). Few measured data deviate from the curve and these may result from igneous activity in East China in the Meso-Cenozoic (Lee et al., 2006; Shinn et al., 2010; Du et al., 2016).

The main uncertainty of the modeling results of tectonothermal evolution lies in the input values of geophysical parameters. Constrained by previous study results (Hao et al., 2010; He, 2002; Liao et al., 2009; Xu et al., 2008, 2009), we first calibrated the stretch factors and current calculated thickness of the crust and compared them with other studies (Bao et al., 2013b; Xu et al., 2008, 2009). Then the key geophysical parameters, including the thickness of initial crust and lithospheric mantle, were determined for subsequent modeling of heat flow trend. Also the trends in HF calculated by numerical modeling were used to calculate *Ro* evolutionary curves to check out the validity of input values by comparing them with the measured data (Fig. 4b).

So this modeling method of integrating geodynamics and geothermometers can effectively enhance the reliability of the modeling results.

4.4 *Analysis of results*

The Meso-Cenozoic thermal evolution processes in the North Subbasin can be divided into three phases (Fig. 4). The initial rifting event occurred during the Middle-Late Jurassic. The thick Jurassic formations that were encountered by the RC20-2-1 well represent strong and rapid subsidence. However, current drilling wells mainly reveal strata since the Cretaceous (Fig. 2). Therefore, by modeling of the tectono-thermal evolution of a single well location it is relatively difficult to reconstruct the history of the tectono-thermal evolution before the Cretaceous. The interpretation of seismic results indicates that Jurassic strata commonly developed in the deep depression area, and their distribution range is significantly smaller than that of the widespread overlying strata (Fig. 2). The results of modeling show that the Cretaceous is a key period when the North Subbasin, in general, entered into a stage of strong rifting and underwent rapid subsidence until the Late Cretaceous, followed by a stage of moderate rifting during the Paleogene. The South Yellow Sea Basin entered into a stage of depression development in the Early Miocene, when rifting mostly ceased.

There is a close relation between syn-rifting tectonic subsidence and the history of thermal evolution (Royden and Keen, 1980; Tong et al., 2005). The results of modeling the history of thermal evolution can be checked against the measured temperature-sensitive parameters. Therefore, an important application of 1D modeling is to calibrate boundary conditions, in particular, to reconstruct the thermal history on the basis of the rapid comparison of results with measured data and then to provide constraints on 3D modeling. The final trend in HF was determined after iterative fitting-based simulations. This process was conducted for well locations (H9 and ZC1-2-1) to obtain the final optimal trend. The final trend in HF matches the measured values of vitrinite reflectance well (Fig. 4). It exhibited a slow increase from an average level of 61 mW/m^2 during the Middle-Late Jurassic, which represents the initial rifting phase of the North Subbasin. Then, the value of HF underwent a strong increase and reached an average value of about 80 mW/m^2 from circa 145 Ma to circa 74 Ma. The rapid thermal subsidence indicates the syn-rifting phase of evolution of the basin. The peak value of HF was followed by a gradual decline to an approximate value of 65 mW/m^2 until the end of the Oligocene, which represents the post-rifting phase. Subsequently, in the depression phase, thermal subsidence nearly ceased and the HF maintained a constant value of 65 mW/m^2. By contrast, the HF trend of north subbasin of the South Yellow Sea is the same as the south subbasin, however, the overall value of the north subbasin is relatively lower than the south subbasin (Yang et al., 2003a, b).

5 Preliminary 3D modeling of the basin

5.1 *3D input*

In PetroBuilder 3-D, a numerical model is established according to the stratigraphic framework, lithologies, facies, and source rock properties. On the basis of data from the BHH, a well-defined conceptual model of the framework of basin filling can be established. The conceptual model is an integrated quantified framework with all parameters or inputs defined (Welte and Yalçin, 1987; Wygrala, 1988). This step requires proper inputs of the stratigraphic framework and related chronostratigraphy, geological events of deposition and erosion, and the creation and basic attributes of faults, as well as definitions of the petroleum system (e.g., the source rock, carrier layer, seal layer, and reservoir rock) and related parameters. Several key input elements that have a significant influence on the results of modeling are discussed as follows.

5.1.1 *Physical stratigraphic framework of the basin*

The evolution of a basin includes sequential geochronological units (events), which represent different time spans during which either deposition, non-deposition, or erosion occurred (Wygrala, 1988; Poelchau et al., 1997). Sedimentary units and/or defined layers that resulted from different geological events constitute the physical stratigraphic framework of the basin. Reasonable constraints on the physical stratigraphic framework are therefore the most important means of control of basin modeling (Poelchau et al., 1997).

In the study area, the thickness of six stratigraphic layers was derived from 2-D seismic data and constrained by well ties. Seven surface maps (surface, Bot_N+Q, Bot_E_{S+D}-1, Bot_E_{S+D}-2, Bot_E_F, Bot_K and Bot_J) were calculated and created using the Petrel software, and the lateral grid size of the initial model was 500 m×500 m. The lateral grid density was completely adequate to satisfy the requirements of the assignment of facies. In contrast, the vertical subdivision of the stratigraphic column is difficult to achieve. Although constrained by seismic surveys, the method of sequence stratigraphy is applicable to subdivisions because it is useful for estimating the vertical sedimentary cycle (Brown and Fisher, 1977; Posamentier and Vail, 1988). Other fundamental principles of subdivision are listed as follows: (1) the layers that can be subdivided should represent a uniform stratigraphic sequence and not contain regional hiatuses or unconformities; (2) regional representative sublayers that are of great significance for petroleum systems, i.e., source sublayers, reservoir sublayers, and seal sublayers, should be reasonably subdivided to assign geophysical and/or geochemical properties to related vertical units; (3) sedimentary facies should be the most important reference point for the subdivision of sublayers because the facies is associated with the petrofacies and has a strong relation with properties related to modeling input such as porosity, permeability, thermal conductivity, PWD, and SWIT; and (4) the number of sublayers should consider the simulation time and computer processing ability.

In immature exploration basins, the subdivision of sublayers is essential to fill data gaps in physical stratigraphy because of sparse subsurface data. Taking the E_F strata as an example, this formation can be divided into four groups, namely, a first group (E_F1), second group (E_F2), third group (E_F3), and fourth group (E_F4), on the basis of the study of sedimentary facies and regional geological analogies (Cai et al., 2014; Zhang et al., 2014a) (Fig. 5). E_F1 is characterized as a sand/shale interbedded series; the lower part is dominated by sandstone, whereas the upper part is mainly brown mudstone. To distinguish the lower fluvial sandstone and the upper lacustrine brown mudstone well, the E_F1 group is subdivided into four sublayers (Fig. 5). Then, the detailed sublayers can allow a more reasonable definition of the physical properties of the lithostratigraphic groups (Poelchau et al., 1997). In the same way, other representative sublayers, such as thick lacustrine dark mudstone, regionally compacted shale, and thick sandstone, are also subdivided and extracted for more reasonable assignment. In total, 18 sublayers have been subdivided from the E_F. In the North Subbasin, the thickness of the E_F can reach 550 m and the average thickness of each sublayer is

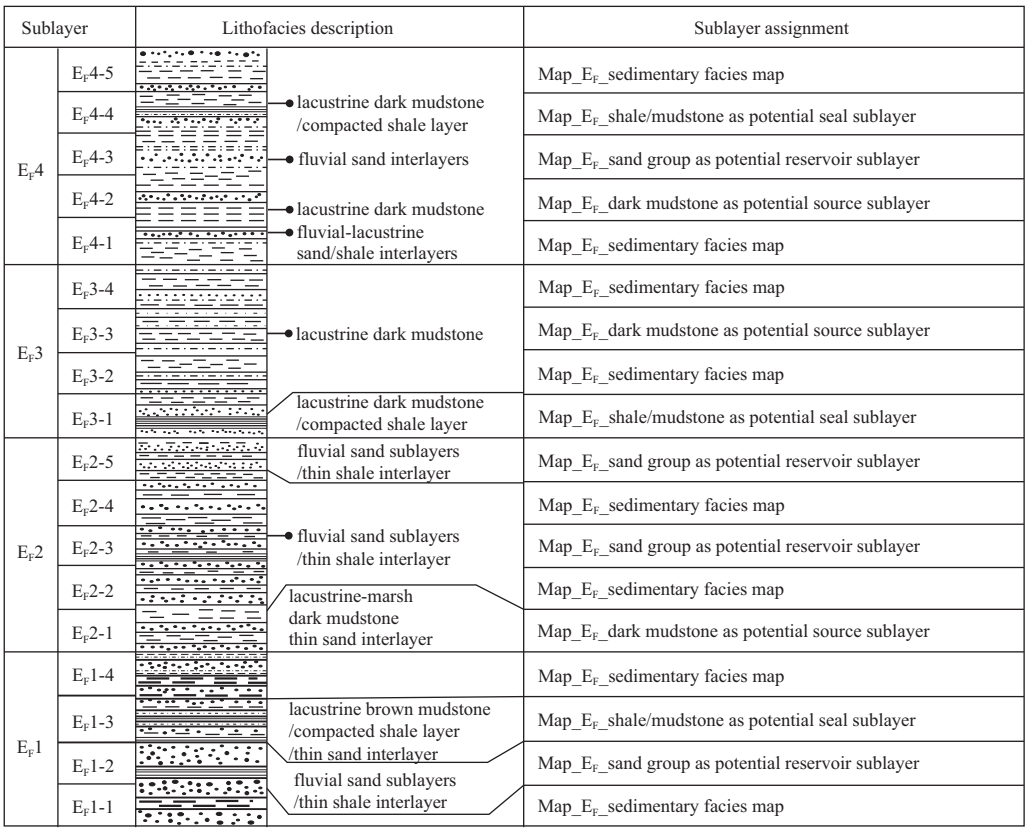

Fig. 5. Analysis of the sedimentary facies, subdivision of sublayers, and related assignment of the Paleogene Funing Formation.

about 30 m.

On account of the processing requirements and accuracy of the simulation, the six resulting layers have been subdivided into 56 sublayers to account for the physical stratigraphic framework of the basin. Two intersecting sections with the assignment of facies are shown in Fig. 6.

5.1.2 *Modeling and properties of faults*

Fault systems are a key controlling factor of the migration, accumulation, and preservation of petroleum (Moretti, 1998; Aydin, 2000; Jin et al., 2008). A spatial model can be created that is based on raw faultline maps of different surfaces (Bot_N+Q, Bot_E_{S+D}-1, Bot_E_{S+D}-2, Bot_E_F, Bot_K and Bot_J). There are a total of 46 faults in the modeling range. With reference to the interpretation of seismic results and vertical subdivisions of the stratigraphic column, each fault model is extended past the respective tip by about 15–150 m, which represents the thickness of one or two sublayers (Fig. 7). The gridded fault model comprises zigzag lines along cells; thus, detailed vertical subdivisions can acquire smoother and more continuous fault planes (Fig. 7).

In the North Subbasin, it is difficult to define the integral properties of the faults. However, the fault activity period, which is an essential constraint for simulations, has been analyzed. Because the rift evolution of a basin has a strong relation to the subsidence rate, the results of 1-D modeling of the burial history should be an important reference point for the definition of the fault activity period of adjacent syn-rifting faults. The structural analysis of the intersecting relation between fault planes and tectonic surfaces is significant for determining the development stage of secondary faults and small faults. In addition, the results of research into regional stress fields and basin rift evolution processes provided some constraints for the definitions of fault properties. Three types of fault have been classified according to their active periods: (1) Type I is syn-rifting faults, and their active period commenced from the Middle-Late Jurassic and ceased in the Early Miocene; (2) Type II is syn-rifting secondary faults, and their active periods are defined by the time spans of intersecting strata intervals; and (3) Type III is a few continuously active faults, which can extend upward to the Neogene strata.

5.1.3 *Source rocks*

Source rocks can be assigned by maps of sedimentary facies and dark mudstone sublayers (Section 5.1.1; Fig. 6). In the first case, the lacustrine mudstones, which have been selected as corresponding parameters for evaluation on the basis of drilling data, are relatively reliable source rocks. However, when assigned by the presence of dark mudstone sublayers, the distribution range of source rocks is apparently too large and should be constrained by the use of maps of sedimentary facies. Moreover, some lacustrine red/brown mudstones cannot act as source rocks, and the respective gridding cells should not be assigned source rock parameters. For example, the Cretaceous strata in the northeastern segment are characterized by red clastic strata, and all the cells that were assigned as K-lacustrine mudstone in the northeastern segment have been selected and the corresponding source rock parameters have been removed.

The parameters used for the evaluation of source rocks are mainly derived from the measured data from drilling cores. The conventional model of hydrocarbon generation is based on the classification of typical kerogen types (Types I, II, and III). It is supposed that the kinetics model of each type is similar. In this study, the kerogen kinetics model employed for the source rocks

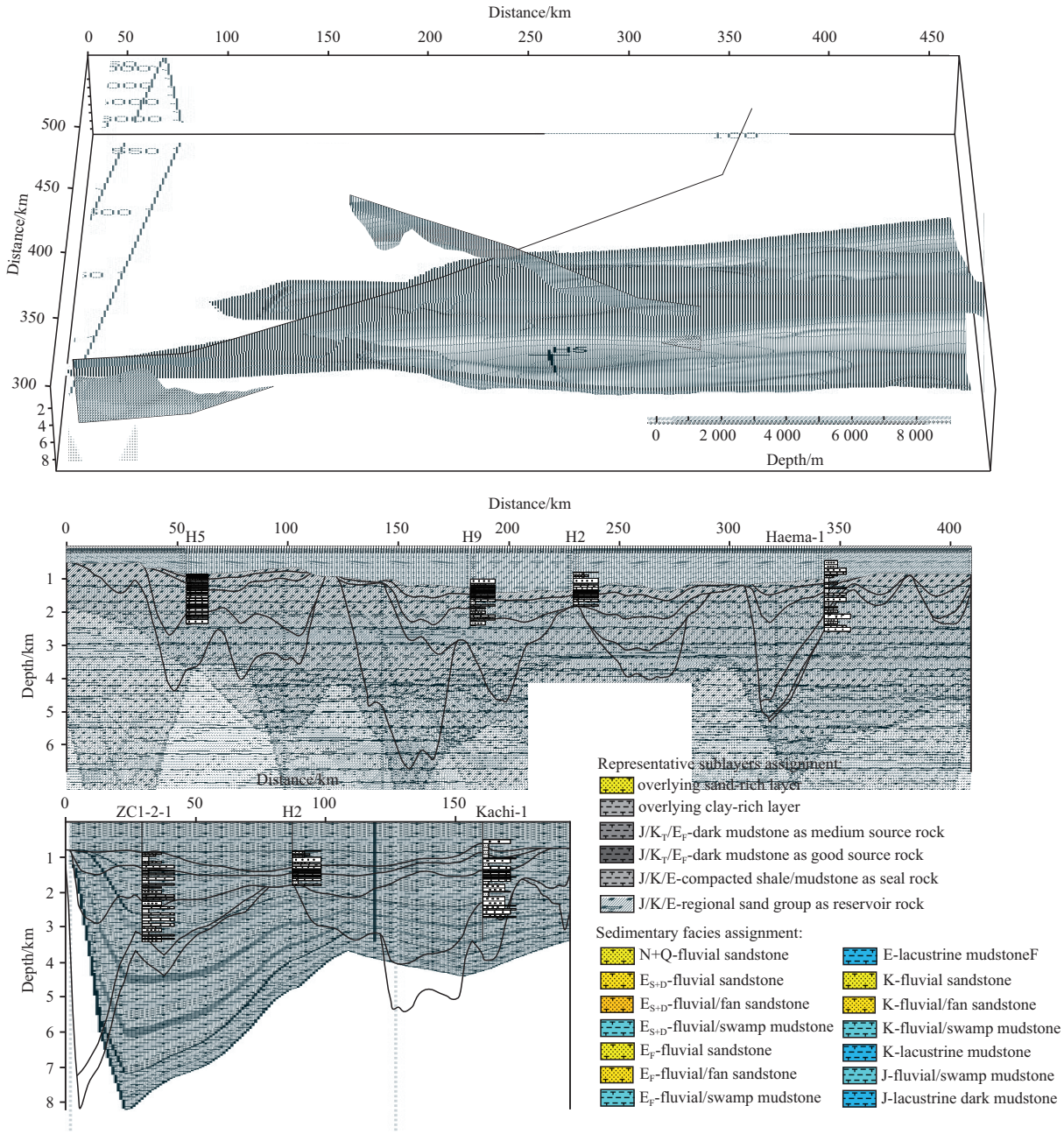

Fig. 6. 3-D model and two intersecting profiles showing the physical stratigraphic framework and subdivision into sublayers. Drilling wells that have been projected onto the profiles are used to confirm the subdivisions and assignments.

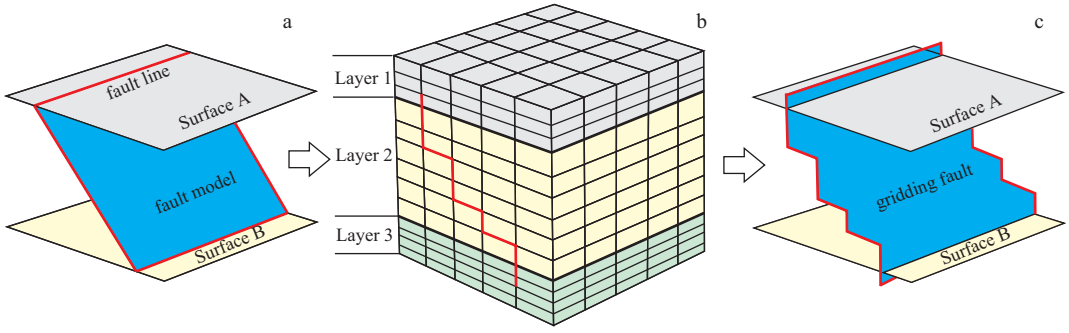

Fig. 7. A simple fault model is created from two fault lines on Surfaces A and B (a). Gridding cells (b) and gridding fault (c), the quality of the gridding fault (c) has a close relation to the density of the gridding cells (b).

in the Jurassic, Cretaceous, and Paleogene strata in the study area utilized pyrolysis kinetics (kerogen Types II and III) based on the findings of Behar et al. (1997).

5.1.4 *Boundary conditions*

The map of the PWD was based on the analysis of sedimentary facies and was generally in accordance with the map of individual facies. The SWIT was calculated automatically from the global mean surface temperature, as described for 1-D modeling (Section 4.2). The values of HF were mapped on the basis of the trends derived from the results of 1-D modeling (Section 4.1). With reference to the typical values of HF for sedimentary basins in similar tectonic situations (Juan, 1986; Allen and Allen, 1990), the range of values in HF maps of this area was constrained from 50 to 120 mW/m^2.

5.2 *Results for the petroleum system*

Abundant data and maps covering the maturation of organic matter and generation, expulsion, migration, and accumulation of hydrocarbons can be obtained from the results of 3-D modeling. The geodynamic processes in the petroleum system can be reconstructed. The results of modeling of vitrinite reflectance show that the source rocks in and below the E_F are mature (Fig. 8), which is in accordance with the measured data and the results of 1-D modeling (Cao and Ye, 2008; Cao et al., 2009) (Fig. 4). The maximum value (*Ro*(%)) in the E_F can reach 0.8% at the depocenter, but most values are generally near the threshold of 0.5% (Figs 4 and 8). The Paleogene Sanduo and Dainan formations (E_{s+d}), however, hardly reach the threshold for hydrocarbon generation. The results of modeling also indicate that, at present, the majority of Jurassic and Cretaceous source rocks in the North Subbasin have reached or exceeded peak oil generation and most source rocks have completed the generation and expulsion of oil. The burial depth of Jurassic source rocks can reach 8 000 m at the depocenter (Segments A and C; Figs 1 and 6), and the results of modeling of vitrinite reflectance (*Ro*(%)) can reach 3.5% (Fig. 8). However, it should be noted that the distribution of Jurassic source rocks is still uncertain.

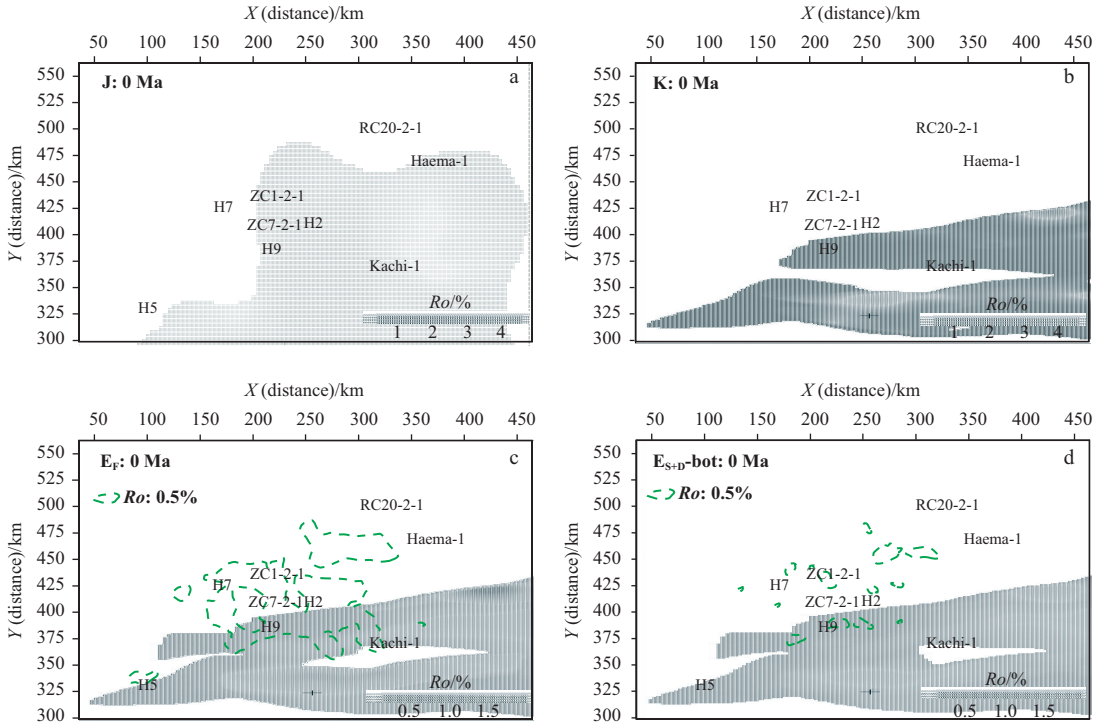

Fig. 8. Results of modeling of vitrinite reflectance (*Ro*(%)) at 0 Ma, showing the maturity of the source rocks in the J/K/E_F/E_{S+D}–bot strata intervals.

The results reveal that the main generation and expulsion in Jurassic source rocks took place during the syn-rifting and post-rifting phases, whereas peak generation and expulsion in Cretaceous and Paleogene source rocks took place during the post-rifting phase (Figs 3 and 9). Generation was dominated by thermal subsidence. When controlled by abundant active faults, petroleum can be expelled immediately after generation, showing a good relation between generation and expulsion on the time axis. The area yields for generation and expulsion (Mt/km^2) are correspondingly controlled by depocenters during the initial rifting and syn-rifting phases. In general, the efficiency of hydrocarbon expulsion is relatively high, particularly in Jurassic source rocks, and the average value is about 90%. Statistical histograms of the generation and expulsion rates of different strata intervals are shown in Fig. 9.

Flow path simulations demonstrate that most oil and gas accumulations in the North Subbasin surround depocenters and are situated close to the modeled migration pathways (Fig. 10). Flow paths originate from deep depocenters, extend along structural ridges and faults, and then pass through or terminate in pools. The basin boundary is open in the simulation process, which leads to some losses of hydrocarbons by pathways that connect to the basin margin. The results of accumulations and possible flow paths at different times show that oil and gas generated during the Jurassic and the Early Cretaceous were almost lost from the basin margin and some deep active faults. However,

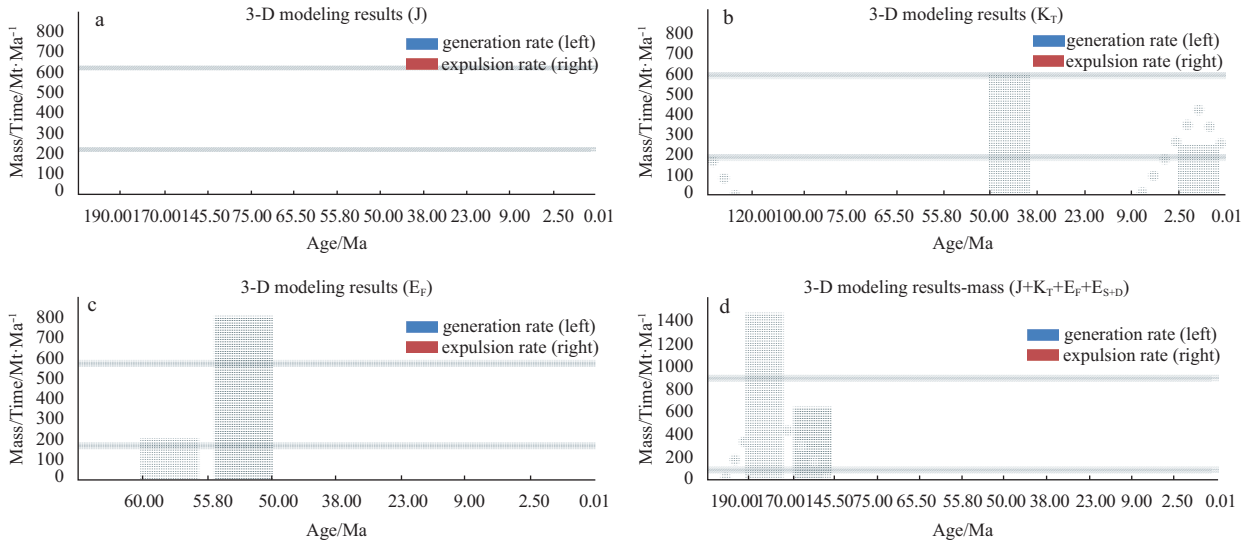

Fig. 9. Statistical histograms of the generation and expulsion rates of different strata intervals (J/K_T/E_F/mass) from the results of 3-D modeling.

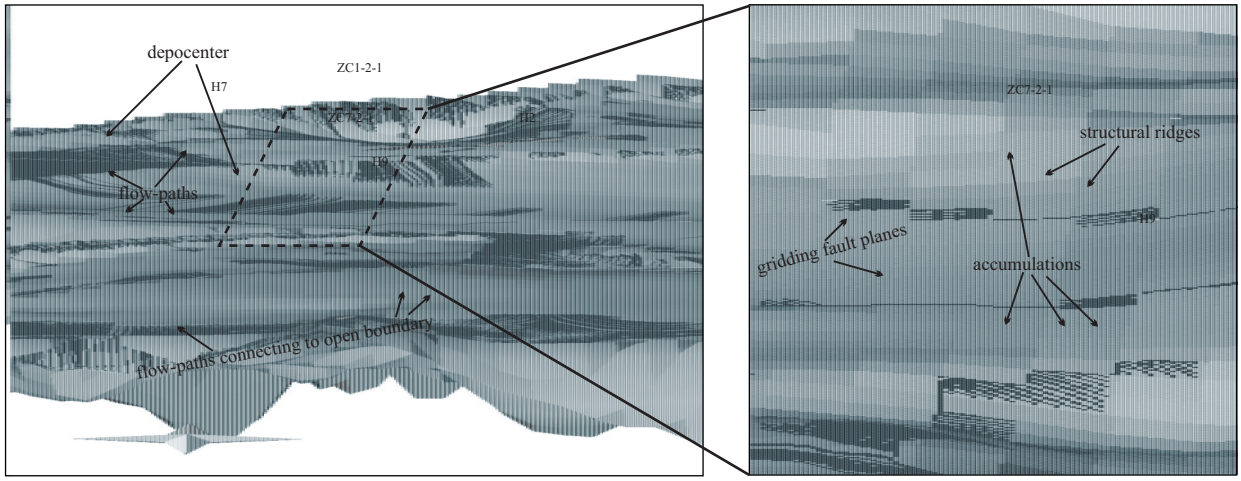

Fig. 10. Segmental results of 3-D simulations with oil and gas accumulations and flow paths.

there are still a considerable number of residual accumulations present in the structurally uplifted areas around the depocenter. According to the density of flow paths and accumulation sites, dominant migration pathways can be predicted.

5.3 *Evaluation of results of 3-D modeling*

Because of the complexity of the petroleum system, corresponding geodynamic processes, and limited amount of data available from the basin, which has been explored to a limited degree, some fundamental conditions that have a major influence on the results of modeling are still uncertain. First, the interpretation of tectonic data, such as maps of layers and fault lines, almost all of which are derived from multichannel seismic data, is unclear. There are 56 sublayers that have been subdivided in the final model of the stratigraphic framework; however, only seven surface maps and a few wells are available to provide data to constrain the subdivisions (Fig. 2). In particular, the deep Jurassic strata, which have been drilled through up to a thickness of over 2 000 m by the RC20-2-1 well, appears to be the most important petroleum-generating layer according to the results of modeling, contributing to nearly half of the gross volume of the basin. Regrettably, the bottom surface of the Jurassic (Bot_J) still lacks sufficient supporting data. Second, the development and activity periods of faults control the expulsion and migration of petroleum to a great extent and have a significant influence on the vertical distribution of petroleum accumulations. Figure 10 shows that the flow paths and accumulations have closely linked relations to the gridded fault lines. The fault spatial models and related gridding processes can be reasonably constrained for the requirements of simulations (Fig. 7). However, the properties of the faults, as discussed in Section 5.1.2, still lack credible constraints. Once the physical stratigraphic framework and assignment of facies are completed, the reservoirs where oil and gas finally accumulate are mainly dominated by the definition of the properties of faults according to the results of multiple simulations. The multiple simulations based on a single-factor analysis are an effective approach to ranking uncertainty factors. However, it is essential to merge the gridding cells to decrease the simulation time, which will correspondingly influence the accuracy of the simulation results. Third, the maturity of the E_F and E_{S+D} is generally near the threshold (Fig. 8). They are therefore sensitive to the history of thermal evolution and related parameters. The

simulation results of thermal evolution history have been checked against calibration parameters and, if necessary, the related inputs have also been modified to obtain a better match between the simulated and measured data. We compared the modeling results of the petroleum system with the results of previous studies and observed that hydrocarbon potential and expulsion have the same order of magnitude as that obtained in the previous resource evaluation results (Xiao, 2002). However, a difference in the hydrocarbon accumulation was observed. The accumulation obviously changes each time the key parameters, particularly the faults properties, are adjusted. Although the South Yellow Sea Basin is still in the initial stage of exploration, basin modeling is an efficient approach for the evaluation and exploration of basin resources.

6 Conclusions

Basin modeling is an effective approach for analyzing sedimentary basins and can provide a comprehensive evaluation of a petroleum system. The modeling of tectono-thermal evolution and preliminary 3-D basin modeling have been introduced and performed in the North Subbasin of the South Yellow Sea Basin. The conclusions are as follows.

(1) The trend in HF has been reconstructed and calibrated via modeling of tectono-thermal evolution. The final optimal trend commenced from an average level of 61 mW/m^2 during Middle-Late Jurassic, experienced a strong increase to reach about 80 mW/m^2 from circa 145 Ma to circa 74 Ma, and then underwent a gradual decline to an approximate value of 65 mW/m^2 until the end of Oligocene.

(2) Three evolutionary phases, namely, an initial rifting phase, a syn-rifting phase, and a post-rifting phase, have been identified on the basis of the reconstruction of burial and thermal history. The Cretaceous is a key period when the North Subbasin in general entered into a stage of strong rifting and underwent rapid subsidence until the Late Cretaceous, followed by a stage of moderate rifting during the Paleogene.

(3) Preliminary results of 3-D modeling reveal that the maturity of source rocks in the E_F is generally near the threshold, the deep Jurassic and Cretaceous source rocks have reached or exceeded peak oil generation, and most source rocks have completed the generation and expulsion of hydrocarbons. Controlled by a history of the thermal subsidence, the main generation and expulsion in Jurassic source rocks took place during the syn-rifting and post-rifting phases, whereas the peak generation and expulsion in the Cretaceous and Paleogene source rocks took place during the post-rifting phase.

(4) The South Yellow Sea Basin is still a relatively less explored sedimentary basin. There are still some uncertainties that have a significant influence on the results of modeling, according to the analysis of the modeling processes and results.

Acknowledgements

Database for basin modeling is supported by Qingdao Institute of Marine Geology (QIMG), China. We thank Duan Jing from Missouri University of Science and Technology for revising the manuscript.

References

Allen P A, Allen J R. 1990. Basin analysis: principles and applications. Cambridge: Blackwell Scientific Publications, 451

Aydin A. 2000. Fractures, faults, and hydrocarbon entrapment, migration and flow. Marine and petroleum geology, 17(7): 797–814

Bao Hanyong, Guo Zhanfeng, Huang Yaping, et al. 2013a. tectono-thermal evolution of the Subei Basin since the Late Cretaceous. Geological Journal of China Universities (in Chinese), 19(4): 574–579

Bao Hanyong, Guo Zhanfeng, Zhang Luolei, et al. 2013b. Calculating methods and assessment of stretching factor: a case study of Northern Jiangsu Basin. Petroleum Geology & Experiment (in Chinese), 35(3): 331–346

Baur F, Littke R, Wielens H, et al. 2010. Basin modeling meets rift analysis–A numerical modeling study from the Jeanne d'Arc basin, offshore Newfoundland, Canada. Marine and Petroleum Geology, 27(3): 585–599

Behar F, Vandenbroucke M, Tang Y, et al. 1997. Thermal cracking of kerogen in open and closed systems: determination of kinetic parameters and stoichiometric coefficients for oil and gas generation. Organic Geochemistry, 26(5): 321–339

Brown LF, Fisher WL. 1977. Seismic stratigraphic interpretation of depositional systems. In: Payton CE (ed) Seismic stratigraphy-applications to hydrocarbon exploration. AAPG Mem 26: 213–248

Cai Jia, Zhao Zhigang, Zhang Xilin, et al. 2014. On sedimentary facies in Funing formation of northern sag in north depression in South Yellow Sea Basin. Journal of Geology (in Chinese), 38(4): 530–535

Cao Qiang, Ye Jiaren. 2008. Prediction of source rock of Northeast Sag in North Depression in South Yellow Sea Basin. Geological Science and Technology Information (in Chinese), 27(4): 75–79

Cao Qiang, Ye Jiaren, Shi Wanzhong, et al. 2009. Preliminary prediction and evaluation of source rocks in low-exploration basins: A case study on the northeast sag of the Northern South Yellow Sea Basin in China. Acta Petrolei Sinica (in Chinese), 30(4): 522–529

Du Qingxiang, Han Zuozhen, Shen Xiaoli, et al. 2017. Geochemistry and geochronology of Upper Permian–Upper Triassic volcanic rocks in eastern Jilin Province, NE China: implications for the tectonic evolution of the Palaeo-Asian Ocean. International Geology Review, 59(3): 368–390

Gao Shunli, Xu Xi, Zhou Zuyi. 2015. Structural deformation and genesis of the northern sub-basin in South Yellow Sea since Late Cretaceous. Oil & Gas Geology (in Chinese), 36(6): 924–933

Gao Shunli, Zhou Zuyi. 2014. Discovery of the Jurassic strata in the North-East Sag of South Yellow Sea. Geological Journal of China Universities (in Chinese), 20(2): 286–293

Gonçalves F T, Mora C A, Córdoba F, et al. 2002. Petroleum generation and migration in the Putumayo Basin, Colombia: insights from an organic geochemistry and basin modeling study in the foothills. Marine and petroleum geology, 19(6): 711–725

Hao Tianyao, Huang Song, Xu Ya, et al. 2010. Geophysical understandings on deep structure in Yellow Sea. Chinese Journal of Geophysics (in Chinese), 53(6): 315–1326

He Lijuan. 2002. Effects of lithospheric rheology on thermal-mechanical modeling of extensional basins. Chinese Journal of Geophysics (in Chinese), 45(1): 49–55

Helwig J A. 1985. Origin and classification of sedimentary basins. 17th Annu offshore TechnolConf, Houston, OTC 4843, 21–32.

Hou Fanghui, Zhang Zhixun, Zhang Xunhua, et al. 2008. Geologic evolution and tectonic styles in the South Yellow Sea Basin. Marine Geology & Quaternary Geology (in Chinese), 28(5): 61–68

Jarvis G T, McKenzie D P. 1980. Sedimentary basin formation with finite extension rates. Earth and Planetary Science Letters, 48(1): 42–52

Jin Zhijun, Cao Jian, Hu Wenxuan, et al. 2008. Episodic petroleum fluid migration in fault zones of the northwestern Junggar Basin (northwest China): Evidence from hydrocarbon-bearing zoned calcite cement. AAPG bulletin, 92(9): 1225–1243

Juan V C. 1986. Thermal-tectonic evolution of the Yellow Sea and East China Sea-Implication for transformation of continental to oceanic crust and marginal basin formation. Tectonophysics, 125(1-3): 231–244

Lee G H, Kwon Y I, Yoon C S, et al. 2006. Igneous complexes in the

eastern Northern South Yellow Sea Basin and their implications for hydrocarbon systems. Marine and Petroleum Geology, 23(6): 631–645

Li Pilong, Jin Zhijun, Zhang Shanwen, et al. 2003. The present research status and progress of petroleum exploration in the Jiyang Depression. Petroleum Exploration and Development (in Chinese), 30(3): 1–4

Li Ming, Zhao Yimin, Liu Xiao, et al. 2009. Distribution of petroleum enriched areas, Changling Sag, southern Songliao Basin. Petroleum Exploration and Development (in Chinese), 36(4): 413–418

Liao Jie, Zhou Di, Zhao Zhongxian. 2009. Numerical models of the tectono-thermal evolution of rift basins and their applications to the Northern South China Sea. Journal of Tropical Oceanography (in Chinese), 28(6): 41–51

Liu Qiongying, He Lijuan. 2015. Discussion on several problems in tectono-thermal modeling of rift basins. Chinese Journal of Geophysics (in Chinese), 58(2): 601–612

Magoon L B, Dow W G. 1994. The petroleum system: From source to trap. American Association of Petroleum Geologists (AAPG), Mem 60, Tulsa: 3–24

McKenzie D. 1978. Some remarks on the development of sedimentary basins. Earth and Planetary science letters, 40(1): 25–32

Moretti I. 1998. The role of faults in hydrocarbon migration. Petroleum Geoscience, 4(1): 81–94

Novelli L, Welte D H, Mattavelli L, et al. 1988. Hydrocarbon generation in southern Sicily. A three dimensional computer aided basin modeling study. Organic geochemistry, 13(1): 153–164

Pang Yumao, Zhang Xunhua, Xiao Guolin, et al. 2016a. Comparative study of tectonic evolution and petroleum geological conditions of typical superimposed basins in upper and lower Yangtze block. Marine Geology & Quaternary Geology (in Chinese), 36(1): 133–142

Pang Yumao, Zhang Xunhua, Xiao Guolin, et al. 2016b. Structural and geological characteristics of the South Yellow Sea Basin in Lower Yangtze Block. Geological Review (in Chinese), 62(3): 604–616

Pang Yumao, Zhang Xunhua, Xiao Guolin, et al. 2017. Characteristics of Meso-Cenozoic Igneous Complexes in the South Yellow Sea Basin, Lower Yangtze Craton of Eastern China and the Tectonic Setting. ACTA GEOLOGICA SINICA(English edition), 91(3): 971–987

Pitman J K, Steinshouer D, Lewan M. 2004. Petroleum generation and migration in the Mesopotamian Basin and Zagros Fold Belt of Iraq: results from a basin-modeling study. GeoArabia, 9(4): 41–72

Poelchau H S, Baker D R, Hantschel T, et al. 1997. Basin simulation and the design of the conceptual basin model. In: Welte D H, Horsfield B, Baker D R, Eds. Petroleum and Basin Evolution. Berlin: Springer, 3–70

Posamentier H W, Vail P R. 1988. Sequences, systems tracts and eustatic cycles. AAPG Bull 72: 237

Qi Jianghao, Wen Zhenhe, Zhang Xunhua, et al. 2013. Lithostratigraphic correlation of Mesozoic and Palaeozoic marine strata between South Yellow Sea and Upper Yangtze region. Marine Geology&Quaternary Geology (in Chinese), 33(1): 109–119

Qiu Nansheng. 2004. Sedimentary basin thermal system research theory and application. Beijing, China, Petroleum Industry Press (In Chinese)

Rodriguez J F, Littke R. 2001. Petroleum generation and accumulation in the Golfo San Jorge Basin, Argentina: a basin modeling study. Marine and Petroleum Geology, 18(9): 995–1028

Royden L, Keen C E. 1980. Rifting process and thermal evolution of the continental margin of eastern Canada determined from subsidence curves. Earth and Planetary Science Letters, 51(2): 343–361

Schneider F, Wolf S, Faille I, et al. 2000. A 3D basin model for hydrocarbon potential evaluation: application to Congo offshore. Oil & Gas Science and Technology, 55(1): 3–13

Shinn Y J, Chough S K, Hwang I G. 2010. Structural development and tectonic evolution of Gunsan Basin (Cretaceous-Tertiary) in the central Yellow Sea. Marine and Petroleum Geology, 27(2): 500–514

Steckler M S, Watts A B. 1978. Subsidence of the Atlantic-type continental margin off New York. Earth and Planetary Science Letters, 41(1): 1–13

Sweeney J J, Burnham A K. 1990. Evaluation of a simple model of vitrinite reflectance based on chemical kinetics (1). AAPG, 74(10): 1559–1570

Tong Zhigang, Hu Gencheng, He Qing. 2005. The tectonic subsidence and heat flow of the Western Nansha area. Geotectonica ET Metallogenia (in Chinese), 29(3): 371–376

Wang Liangshu, Li Cheng, Shi Yangshen, et al. 1995. Distributions of geotemperature and terrestrial heat flow density in Lower Yangtze area. Acta Geophysica Sinica (in Chinese), 38(4): 469–476

Waples D W. 2001. A new model for heat flow in extensional basins: radiogenicheat, asthenospheric heat, and the McKenzie model. Natural ResourcesResearch, 10(3): 227–238

Welte D H, Yalçin M N. 1987. Formation and occurrence of petroleum in sedimentary basins as deduced from computer-aided basin modelling. Petroleum geochemistry and exploration in the Afro-Asian region, : 17–23

Welte D H, Yalçin M N. 1988. Basin modelling: a new comprehensive method inpetroleum geology. Organic Geochemistry, 13(1–3): 141–151

Wu Shiguo, Ni Xianglong, Cai Feng. 2008. Petroleum geological framework and hydrocarbon potential in the Yellow Sea. Chinese Journal of Oceanology and Limnology, 26: 23–34

Wygrala B P. 1988. Integrated computer-aided basin modeling applied to analysis of hydrocarbon generation history in a Northern Italian oil field. Organic geochemistry, 13(1): 187–197

Wygrala B P. 1989. Integrated study of an oil field in the southern Po basin, northern Italy [dissertation]. Germany: University of Cologne

Xiao Guolin. 2002. Reassessment of petroleum geologic features and potential reserves in the South Yellow Sea Basin. Marine Geology & Quaternary Geology (in Chinese), 22(2): 81–87

Xu Yi, Li Zhiwei, Liu Jinsong, et al. 2008. Pn wave velocity and anisotropy in the Yellow Sea and adjacent region. Chinese Journal of Geophysics (in Chinese), 51(5): 1444–1450

Xu Yi, Li Zhiwei, Kim K H, et al. 2009. Crustal velocity structure and collision boundary between the Sino-Korea and Yangtze blocks in the Yellow Sea. Chinese Journal of Geophysics (in Chinese), 52(3): 646–652

Yalçin M N. 1991. Basin modeling and hydrocarbon exploration. Journal of Petroleum Science and Engineering, 5(4): 379–398

Yang Shuchun, Cai Dongsheng, Feng Xiaojie, et al. 2003a. Thermal maturation and hydrocarbon generation stages of the pre-Tertiary source rocks in south basin, the Southern Yellow Sea. China Offshore Oil and Gas: Geology (in Chinese), 17(6): 370–375

Yang Shuchun, Hu Shengbiao, Cai Dongsheng, et al. 2003b. Geothermal field characteristics and tectono-thermal evolution in the southern basin of South Yellow Sea. Chinese Science Bulletin (in Chinese), 48(14): 1564–1569

Yao Yongjian, Chen Chunfeng, Feng Zhiqing, et al. 2010. Tectonic evolution and hydrocarbon potential in northern area of the South Yellow Sea. Journal of Earth Science, 21: 71–82

Yao Yongjian, Feng Zhiqiang, Hao Tianyao, et al. 2008. A new understanding of the structural layers in the South Yellow Sea Basin and their hydrocarbon-bearing characteristics. Earth Science Frontiers, 15(6): 232–240

Yao Yongjian, Xia Bin, Feng Zhiqiang, et al. 2005. Tectonic evolution of the South Yellow Sea since the Paleozoic. Petroleum Geology & Experiment (in Chinese), 27(2): 124–128

Yi S, Yi S, Batten D J, et al. 2003. Cretaceous and Cenozoic non-marine deposits of the Northern South Yellow Sea Basin, offshore western Korea: palynostratigraphy and palaeoenvironments. Palaeogeography, Palaeoclimatology, Palaeoecology, 191(1): 15–44

Zhang Xunhua, Yang Jinyu, Li Gang, et al. 2014a. Basement structure

and distribution of Mesozoic-Paleozoic marine strata in the South Yellow Sea basin. Chinese Journal of Geophysics (in Chinese), 57(12): 4041–4051

Zhang Yinguo, Xiao Guolin, Wu Zhiqiang, et al. 2014b. Sedimentary characteristics and evolution of the Paleogene in the northern depression of the South Yellow Sea Basin. Marine Geology Frontiers (in Chinese), 30(10): 26–33

Zhang Minghua, Xu Deshu, Chen Jianwen. 2007. Geological structure of the yellow sea area from regional gravity and magnetic interpretation. Applied Geophysics, 4(2): 75–83

Zhang Zhongmin, Zhou Jin, Wu Xingwei. 2006. Oil and gas migration periods and accumulation process in central anticlinal zone in the Xihu Sag, the East China Sea Basin. Petroleum Geology & Experiment (in Chinese), 28(1): 30–33

Zhu Ping. 2007. Petroleum system analysis of the Northern Sag, the Southern Yellow Sea Basin. Petroleum Geology & Experiment (in Chinese), 29(6): 549–553